PROCEEDINGS OF SCIENCE

Galactic dark matter constrained by synchrotron emission

Silvia Manconi[a,*]

[a] *Laboratoire d'Annecy-le-Vieux de Physique Théorique (LAPTh), CNRS, USMB, F-74940 Annecy, France*

E-mail: manconi@lapth.cnrs.fr

Dark Matter in our Galaxy may produce a linearly polarized synchrotron signal through the secondary emission of electrons and positrons originating, for example, from dark matter annihilations. Using the latest Planck data release, we use for the first time microwave synchrotron polarization to constrain Dark Matter annihilation in the Galaxy. We demonstrate that polarization is more constraining than synchrotron intensity by about one order of magnitude, independently from uncertainties in the modeling of electron and positron propagation and the model of Galactic magnetic field. We discuss the extension of these constraints to further exotic electron and positron injections in the Galaxy such as primordial black holes, as well as improvements in the modeling of the background emissions coming from Galactic sources.

38th International Cosmic Ray Conference (ICRC2023)
26 July - 3 August, 2023
Nagoya, Japan

ICRC2023
38th International Cosmic Ray Conference
The Astroparticle Physics Conference

*Speaker

PoS(ICRC2023)1441

1. Introduction

Indirect searches for dark matter (DM) in cosmic radiations restlessly exploit the complementarity among messengers, in form of photons or charged particles, of energies from radio to multi-TeV, as well as multiple targets and observables, searching for DM signatures, and constraining the current candidates and their parameter spaces [1]. In this contribution we propose the microwave polarization maps measured by the *Planck* collaboration as new observable to constrain DM annihilation in the Galaxy. The material discussed in this proceeding follows Ref. [2], with some extended discussion on how this approach could be extended further in the future.

Planck has so far provided the deepest and highest-resolution view of the microwave and sub-millimeter sky [3]. The *Planck* instrument measures both the intensity and polarization of the microwave and sub-millimeter sky, in terms of the Stokes components I (intensity) and Q, U (polarization). The polarization amplitude is defined as $P = \sqrt{Q^2 + U^2}$. The *Planck* sky maps contain contributions from the Cosmic Microwave Background (CMB), as well as many other astrophysical components ranging from compact Galactic and extragalactic sources to diffuse backgrounds as synchrotron and free-free emission in our Galaxy, see e.g. Fig.4 in Ref. [3]. An important contribution to the *Planck* sky maps is produced by relativistic $e^{\pm}$ that gyrate and propagate in the interstellar Galactic magnetic field (GMF), and emit secondary emissions such as radio and microwave emission through the synchrotron process. High-energetic Galactic cosmic-ray (CR) electrons *and* positrons ($e^{\pm}$ in what follows) can be either accelerated in primary sources such as supernova remnants and pulsar wind nebulae, or produced by spallation of hadronic CRs. Besides, CR $e^{\pm}$ might also be produced by the annihilation or decay of dark matter (DM) particles in the Galactic DM halo. The synchrotron signal of DM origin has been extensively investigated in the past using many radio and microwave surveys, such as WMAP and *Planck*, finding constraints which are complementary to other probes, see e.g. [4–12]. Previous DM searches focused on the synchrotron total intensity, i.e., the Stokes parameter I. However, synchrotron emission of relativistic $e^{\pm}$ is partially linearly polarized, and a signal in polarization amplitude (i.e., Stokes P) is thus expected. The total intensity and the polarization properties of the DM synchrotron emission depend on the strength and orientation of the GMF, as well as on the spatial and energetic distribution of CR $e^{\pm}$ produced by DM. As we demonstrate in what follows, the synchrotron intensity and polarization signals are complementary, since they are controlled by different properties of the GMF, and are thus affected by different systematic uncertainties.

2. Modeling synchrotron from Galactic dark matter

The source term for $e^{\pm}$ produced from (Majorana fermions) WIMP annihilations in the Milky Way DM halo reads:

$$q_{\mathrm{e}^{\pm}}(\mathbf{x}, E) = \frac{1}{2}\left(\frac{\rho_{\mathrm{DM}}(\mathbf{x})}{m_{\mathrm{DM}}}\right)^2 \Sigma_f \langle\sigma v\rangle_f \frac{dN^f_{e^{\pm}}}{dE} \tag{1}$$

where m_{DM} is the DM mass, $\rho_{\mathrm{DM}}(\mathbf{x})$ is the DM density profile in the Galaxy (assumed to be spherically symmetric), f runs over the considered DM annihilation channels, $\langle\sigma v\rangle$ is the velocity averaged cross section, and $dN^f_{e^{\pm}}/dE$ is the $e^{\pm}$ energy spectrum per annihilation for each annihilation channel f. The DM radial distribution $\rho_{\mathrm{DM}}(r)$ in the Galaxy at distance r from the halo center

can be effectively described by the Navarro-Frenk-White (NFW) and generalized NFW density profile [13], where we fix the scale radius to $r_S = 23$ kpc and enforce the local DM density at the solar position to be $\rho_{\rm DM}(r_\odot = 8.5\ {\rm kpc}) = 0.4\ {\rm GeV/cm^3}$ [14]. We consider standard WIMPs with masses $m_{\rm DM}$ between 5 GeV and 1 TeV annihilating into three representative channels: two leptonic channels, $\tau^+\tau^-$ and $\mu^+\mu^-$, expected to produce more $e^\pm$ in their final states, and one hadronic channel $b\bar{b}$, producing a much softer spectrum. The reference thermally averaged annihilation cross section is $\langle\sigma v\rangle = 3\times10^{-26}\ {\rm cm^3 s^{-1}}$. The $e^\pm$ energy spectrum $dN^f_{e^\pm}/dE$ for each channel is taken from the PPPC4DMID library [15].

We here use `GALPROP` version v54r2766 [16, 17] [1] as adapted in Ref. [11] [2] to numerically solve the 3D propagation of $e^\pm$ in the interstellar medium and predict the all-sky total synchrotron intensity and polarization maps from DM annihilations. As benchmark propagation model, we use the plain diffusion model without convection and reacceleration (named `PDDE`) from [18, 19].

The main systematic uncertainty of the present work is anticipated to be associated to the modeling of the GMF, which is still poorly constrained [20]. We thus rely on past studies which fitted the most updated GMF models to multiwavelength data. To bracket the uncertainties associated to GMF modeling, we consider the following three benchmarks: The Sun+10 model proposed in Refs. [21, 22], the model proposed in Ref. [23] (Psh+11), and the more sophisticated model presented by Jansson & Farrar for the regular [24] and random [25] magnetic fields (JF12). These models differ both for the regular and the random MF component. A crucial observation is the fact that intensity and polarization have a different dependence on the MF. While intensity depends on the total MF (random+ordered), polarization only depends on the regular component. This makes the two probes highly complementary.

3. Planck microwave maps

We are interested in constraining a possible diffuse signal coming from DM annihilation in our Galaxy which, depending on the DM properties, may contribute significantly to the diffuse background. Since the CMB contribution is well-measured, we consider CMB-subtracted maps. We refrain from modeling and subtracting any other contribution from the diffuse backgrounds, such as the Galactic synchrotron emission. We thus derive conservative DM constraints requiring that the DM signal does not exceed the observed emission, once the CMB contribution has been subtracted. We use data products corresponding to the third release by the *Planck* collaboration (PR3) for the low frequency instruments (LFI) at 30, 44 and 70 GHz processed with the NILC method [26]. Regarding the polarization emission, the PR3 maps for each of the three Stokes parameters I, Q, U supersede all previous releases thanks to significantly lower contamination from systematic errors. The maps contain the observed blackbody differential brightness temperature, which is related to the flux $\mathcal{J}_{I,P}(\nu, b, l)$ in units of erg cm^{-2}/s/Hz/sr as:

$$T_{I,P}(\nu) = \frac{c^2 \mathcal{J}_{I,P}}{2\nu^2 k_B}, \tag{2}$$

where ν is the frequency and b, l are galactic coordinates. This is the temperature that a body with a Rayleigh Jeans (RJ) spectrum would need in order to emit the same intensity at a given frequency ν.

[1] publicy available at https://gitlab.mpcdf.mpg.de/aws/galprop
[2] publicy available at https://github.com/a-e-egorov/GALPROP_DM

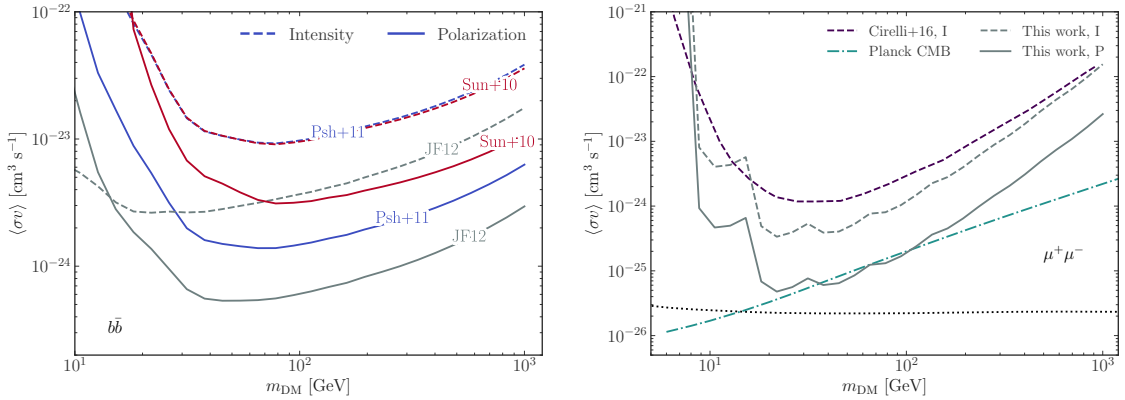

Figure 1: Upper limits on the thermally averaged annihilation cross section as a function of DM mass as derived from the *Planck* intensity (dashed lines) and polarization (solid lines) data at 30 GHz. Left panel: effect of the GMF model for the $\bar{b}b$ channel. Right panel: results for $\mu^+\mu^-$ channel are compared with the analysis of ref. [12] of early *Planck* data at 30 GHz using synchrotron intensity only and CMB limits obtained from *Planck* data [29]. The horizontal dotted line indicates the thermal relic annihilation cross section expectation [30].

Maps are given in units of $K_{\rm CMB}$, which is connected to the Rayleigh-Jeans differential brightness temperature in $K_{\rm RJ}$ by a conversion formula accounting also for color and leakage corrections based on instrument bandpass, see Ref. [27] for more details.

Before comparing the DM predicted P map with observations, we need to build the experimental P map and its error map from the available Q and U maps. This is achieved with three steps: (i) smoothing, (ii) error estimation, (iii) degrading. (i) We first smooth the CMB-subtracted I, Q, U maps with a Gaussian beam of 1 degree FWHM, in order to increase the signal-to-noise ratio and reduce systematic effects caused by beam asymmetries. We then create a polarization amplitude map defined as $P = \sqrt{Q^2 + U^2}$, keeping the original resolution (Nside=1024 in the `HEALPix` pixelization scheme [28]) of the Q, U maps. (ii) For the purpose of obtaining robust DM constraints, we need to build error maps from the I, Q, U maps themselves. We estimate the error at each pixel as the variance of all neighboring pixels up to 0.5 degrees, while sticking to the native NSide resolution. The error map for P is derived from the Q, U error maps using error propagation. (iii) The above maps are degraded to a larger pixel resolution when needed. While this is straightforward for the I, P maps, for the error maps one needs to take into account that the error scales with the pixel size as $\sigma_{\rm P}^l = \sigma_{\rm P}/\sqrt{N_{\rm pix}^{1024}/N_{\rm pix}^l}$ for a generic lower resolution l.

4. Results

We use *Planck* LFI maps at 30 GHz as reference, while we show results using higher frequencies maps in Ref. [2]. For each simulated DM map, i.e., for each DM mass and annihilation channel, we compute an upper bound on the DM annihilation cross section by requiring that the DM intensity or polarization signal at a given frequency does not exceed the observed *Planck* signal *plus* the error estimated before, in this way producing limits at the 68% C.L. We enforce this requirement in each pixel at $|b| < 30$ deg, and we provide the upper limit corresponding to the most constraining pixel.

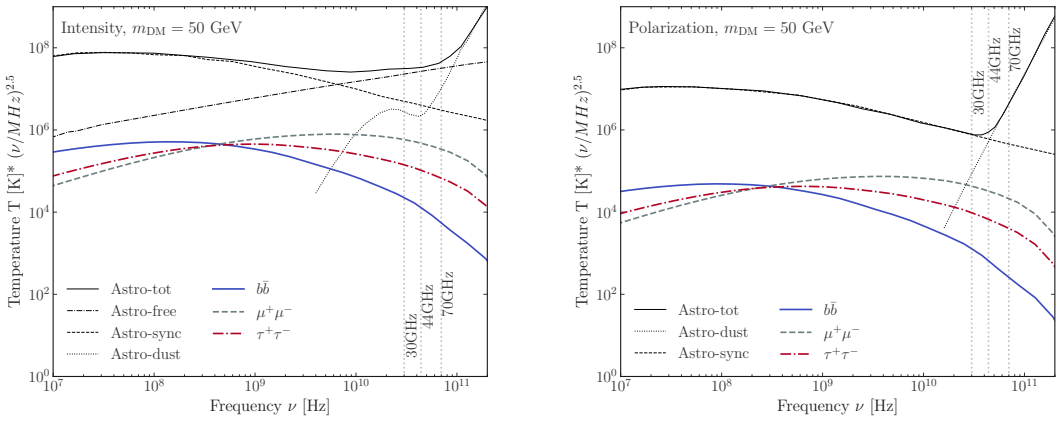

Figure 2: Synchrotron emission spectrum from DM annihilations for total intensity (left panel) and polarization amplitude (right panel) for DM mass of 50 GeV. Vertical dotted lines indicate the frequencies of *Planck* LFI. For all panels the DM signal is computed with `GALPROP` for the line of sight of (l,b)=(20,20)deg, and assuming PDDE propagation parameters, the Psh+11 GMF model and $\langle\sigma v\rangle = 3 \times 10^{-26}$ cm^{3}s^{-1}. The 'Astro' spectra (total, free-free, synchrotron and dust) are taken from a representative model for the intensity and polarization emission at high latitudes which fits multiwavelength data taken from Ref. [17].

Our results for the upper limits obtained using *Planck* intensity and polarization data are illustrated in Fig. 1 (left) for different GMF models and for the $\bar{b}b$ channel and PDDE propagation setup. We have computed also the upper limits for other annihilation channels $\mu^+\mu^-, \tau^+\tau^-$, see Ref. [2]. Results for $\mu^+\mu^-$ are illustrated in the right panel of Fig. 1 for a fixed choice of Psh+11 GMF and PDDE propagation setup. At fixed GMF model, we find that the polarization maps are more constraining than the intensity maps by almost one order of magnitude for DM masses larger than 20 GeV. The Sun+10 and Psh+11 models use the same parametrizations and intensity values for the random field, and thus the intensity constraints are very similar. The random field of the JF12 model has instead a more complicated morphology and a larger strength, which translates into stronger limits by a factor of two. The different morphology and strength for the ordered GMF translate into an uncertainty of about one order of magnitude in the upper limits obtained with the polarization data. The JF12 model is in this case associated to the most stringent upper limits given the non-zero striated component included.

For all the tested channels, the synchrotron polarization data provide constraints at least a factor of five better than the intensity. For different MF this is valid for $m_{\rm DM} > 40$ GeV. At tens of GeV and for $\mu^+\mu^-$ annihilations (Fig. 1, right panel), we exclude $\langle\sigma v\rangle$ larger than about 10^{-25}cm^{3}s^{-1}. This is compared to the thermal relic cross section [30] shown as a dotted line. For the $\mu^+\mu^-$ channel our upper limits using *Planck* polarization are competitive with *Planck* CMB constraints [29] (dot-dashed lines in Fig. 1) between about 50 GeV and 100 GeV.

We interpret the stronger DM constraints from polarization as coming from two effects. First, the astrophysical backgrounds are lower in polarization rather than in the intensity, as illustrated in Fig. 2. We note that the spectrum of the polarization amplitude is very similar to the intensity one, with an overall smaller normalization value at the representative line of sight of (l,b)=(20,20)deg,

at intermediate latitudes in the sky. At *Planck* LFI frequencies, an higher signal is expected in the leptonic channels, in particular in the $\mu^+\mu^-$. The hadronic channels might be better constrained using data at lower frequencies, see e.g. Ref. [12]. We include in Fig. 2 the spectra of the background emissions ('Astro') as estimated in Ref. [17] at high latitudes. Specifically, we take the total astrophysical emission which fits their multiwavelength dataset at high latitudes (right hand plots in their Figure 4), as well as the individual contributions estimated for synchrotron, dust, and free-free emission. For polarization below few tens of GHz, this is just the synchrotron contribution; for intensity, at the WMAP/*Planck* frequencies the free-free and spinning dust contributions are also important. We see that at the *Planck* frequencies the DM polarization signal is a factor 3-4 closer to the astrophysical emission derived in Ref. [17] (which fits the data) with respect to the DM intensity.

Secondly, the intensity and polarization maps have significantly different morphologies. In particular, the polarization map presents filaments, or arms, extending many degrees in the sky (Fig.1 in [2]). This leaves inter-arms regions with very low background very close to the Galactic center, where the DM signal peaks. Instead, the background for the intensity has a more uniform structure towards the inner Galaxy.

4.1 Systematic uncertainties

A careful evaluation of systematic uncertainties affecting our results is available in the supplemental material of Ref. [2]. Specifically, we studied: the effect of pixel size; dark matter density profile; propagation model on the strength of our limits.

With a small pixel size, we are sensitive to the detailed morphology of the signal, but the noise per pixel is large, while with a large pixel we have a smaller noise but we lose the details of the morphology. We find that the constraints are optimized for a choice of an NSide=128, that we adopt as benchmark.

To estimate the uncertainties related to the DM radial distribution, particularly relevant for the innermost part, we consider two additional profiles apart for the standard NFW: a generalized NFW (gNFW) profile with $\gamma > 1$, which can accomodate baryonic effects in simulations of cold DM with $\gamma = 1.25$ and $r_S = 27.2$ kpc, and a cored Burkert profile, with $r_s = 12.67$ kpc. We find that the systematic uncertainty connected to the choice of the DM radial density profile is about one order of magnitude for both intensity and polarization. This is expected, since the constraining power of our analysis comes from the Galactic center region, where the DM signal peaks, and in this region the different choices of profile differ significantly giving large differences in the predicted DM signal.

To gauge the uncertainties related to propagation we consider three propagation models taken from the literature: the benchmark `PDDE`, a model with diffusive reacceleration from the same Refs. [18, 19] (named `DRE`), and a model with convection (named `BASE`) from the recent Ref. [31]. Overall, the systematic uncertainty related to propagation effects is at the level of 20-30% for DM masses above 30 GeV.

5. Summary and Outlook

This contribution presents a new method to constrain DM properties using for the first time as observable the map of CMB foreground polarization. We have derived new, conservative (i.e.,

removing only the CMB) DM constraints using *Planck* synchrotron microwave polarization sky maps. We obtain bounds on the WIMP annihilation cross-section, finding that polarization maps provide DM limits up to one order of magnitude stronger than the ones coming from intensity maps.

Our conservative analysis is the first step towards a more detailed assessment of the constraining power of polarization data. In fact, the DM bounds could be straightened by a proper removal of astrophysical foregrounds on top of the CMB background, and by a more accurate modeling of the GMF and of the DM density profile. Polarization data have been used together with total intensity data to study Galactic synchrotron emission and constrain CR propagation and large scale GMF models in absence of DM annihilation, see e.g. [17, 18, 27]. An example of these results is illustrated in Fig. 2, where the astrophysical model of Ref. [17] is compared to the DM-induced signal. By comparing the two contributions, is evident that potentially stronger constraints can be derived by modeling and subtracting the astrophysical Galactic synchrotron emission within the same framework. However, this assesment should proceed with great care. In fact, we recall that the strength of the GMF is highly degenerate with the normalization of the CR $e^{\pm}$ density in the Galaxy. Additionally, the strength of the GMF is significantly impacting the DM limits as illustrated in Fig. 1. Therefore, a consistent assessment of the parameters of the GMFs should contextually fit also the CR $e^{\pm}$ injection and propagation parameters. We leave this assessment to future work.

We have considered WIMPs as benchmark DM candidates, and we concentrate on the annihilation signal. However, our method could be generalized to other types of particles with electromagnetic annihilation or decay products. Specifically, the approach presented here could be extended to any search for DM or other exotic particles if they inject $e^{\pm}$ in the interstellar medium through annihilation and/or decay processes. One notable example are evaporating primordial black holes with masses of 10^{-18}-10^{-15} solar masses, which are however strongly constrained by MeV and GeV gamma-ray observations [32].

Finally, we note that our method could be extended in the next future using more sensitive observations of the polarized millimeter sky, which should be delivered by the LiteBird satellite [33] or the Simons Observatory [34].

I acknowledge the European Union's Horizon Europe research and innovation programme for support under the Marie Sklodowska-Curie Action HE MSCA PF–2021, grant agreement No.10106280, project VerSi.

References

[1] R. Alves Batista et al., *EuCAPT White Paper (2021), arXiv:2110.10074* (2021).

[2] Silvia Manconi, Alessandro Cuoco, and Julien Lesgourgues, *Phys. Rev. Lett.* **129**(11), pp. 111103 (2022).

[3] N. Aghanim et al., *Astron. Astrophys.* **641**, pp. A1 (2020).

[4] P. Blasi, A. V. Olinto, and C. Tyler, *Astropart. Phys.* **18**, pp. 649–662 (2003).

[5] Dan Hooper, *Phys. Rev. D* **77**, pp. 123523 (2008).

[6] E. Borriello, A. Cuoco, and G. Miele, *Phys. Rev.* **D79**, pp. 023518 (2009).

[7] Marco Regis and Piero Ullio, *Phys. Rev. D* **80**, pp. 043525 (2009).

[8] Timur Delahaye et al., *Mon. Not. Roy. Astron. Soc.* **422**, pp. L16–L20 (2012).

[9] Nicolao Fornengo, Roberto A. Lineros, Marco Regis, et al., *JCAP* **2012**(1), pp. 005 (2012).

[10] Torsten Bringmann et al., *Phys. Rev. D* **90**(12), pp. 123001 (2014).

[11] Andrey E. Egorov, Jennifer M. Gaskins, Elena Pierpaoli, et al., *JCAP* **03**, pp. 060 (2016).

[12] Marco Cirelli and Marco Taoso, *JCAP* **1607**(07), pp. 041 (2016).

[13] Julio F. Navarro et al., *Mon. Not. Roy. Astron. Soc.* **402**, pp. 21 (2010).

[14] Pablo F. de Salas and Axel Widmark, *Rept. Prog. Phys.* **84**(10), pp. 104901 (2021).

[15] Marco Cirelli et al., *JCAP* **03**, pp. 051 (2011), [Erratum: JCAP 10, E01 (2012)].

[16] A. W. Strong, E. Orlando, and T. R. Jaffe, *Astronomy & Astrophysics* **534**, pp. A54 (2011).

[17] Elena Orlando and Andrew Strong, *Mon. Not. Roy. Astron. Soc.* **436**, pp. 2127 (2013).

[18] E. Orlando, *MNRAS* **475**(2), pp. 2724–2742 (2018).

[19] E. Orlando, *Phy. Rev. D* **99**(4), pp. 043007 (2019).

[20] Tess R. Jaffe, *Galaxies* **7**(2), pp. 52 (2019).

[21] X. H. Sun, W. Reich, A. Waelkens, et al., *Astron. Astrophys.* **477**, pp. 573 (2008).

[22] Xiao-Hui Sun and Wolfgang Reich, *Research in Astronomy and Astrophysics* **10**(12), pp. 1287–1297 (2010).

[23] M. S. Pshirkov, P. G. Tinyakov, P. P. Kronberg, et al., *ApJ* **738**(2), pp. 192 (2011).

[24] Ronnie Jansson and Glennys R. Farrar, *Astrophys. J.* **757**, pp. 14 (2012).

[25] Ronnie Jansson and Glennys R. Farrar, *Astrophys. J. Lett.* **761**, pp. L11 (2012).

[26] Y. Akrami et al., *Astron. Astrophys.* **641**, pp. A4 (2020).

[27] Planck Collaboration, *A&A* **596**, pp. A103 (2016).

[28] K. M. Górski, E. Hivon, A. J. Banday, et al., *Astrophys. J.* **622**, pp. 759–771 (2005).

[29] N. Aghanim et al., *Astron. Astrophys.* **641**, pp. A6 (2020), [Erratum: Astron.Astrophys. 652, C4 (2021)].

[30] Gary Steigman, Basudeb Dasgupta, and John F. Beacom, *Phys. Rev. D* **86**, pp. 023506 (2012).

[31] Michael Korsmeier and Alessandro Cuoco, *Phys. Rev. D* **103**(10), pp. 103016 (2021).

[32] Anne M. Green and Bradley J. Kavanagh, *J. Phys. G* **48**(4), pp. 043001 (2021).

[33] M. Hazumi et al., *Proc. SPIE Int. Soc. Opt. Eng.* **11443**, pp. 114432F (2020).

[34] Peter Ade et al., *JCAP* **02**, pp. 056 (2019).